The Nansen Environmental and Remote Sensing Center

a non-profit research institute affiliated with the University of Bergen

Edv. Griegsvei 3a, N-5059 Bergen Norway

NERSC Technical Report no. 243

A possible coupling between the Arctic freshwater, the Arctic sea ice cover and the North Atlantic drift. A case study

by

Odd Helge Otterå and Helge Drange

October 9, 2003

Contents

Abstract

Model studies point to enhanced warming and to increased freshwater fluxes to high northern latitudes in response to global warming. In order to address possible feedbacks in the ice-ocean system in response to such changes, the combined effect of increased freshwater input to the Arctic Ocean and Arctic warming, the latter manifested as a gradual melting of the Arctic sea ice, is examined using a 3-D isopycnic coordinate ocean general circulation model (OGCM). A suite of three idealized experiments is carried out: One control integration, one integration with a doubling of the modern Arctic river runoff, and a third more extreme case, where the river runoff is five times the modern. In the two freshwater cases, the sea ice thickness is reduced by 1.5–2 m in the central Arctic Ocean over a 50 years period.

The modelled ocean response is qualitatively the same for both perturbation experiments: Fresh water propagates into the Atlantic Ocean and the Nordic Seas, leading to an initial weakening of the North Atlantic Drift (NAD). Furthermore, changes in the geostrophic currents in the central Arctic and melting of the Arctic sea ice lead to an intensified Beaufort Gyre (BG), which in turn increases the southward volume transport through the Canadian Archipelago (CA). To compensate for this southward transport of mass, more warm and saline Atlantic water (AW) is carried northward with the NAD. It is found that the increased transport of salt into the northern North Atlantic and the Nordic Seas tend to counteract the impact of the increased freshwater originating from the Arctic, leading to a stabilization of the NAD.

1 Introduction

It is believed that the transport of freshwater into the high northern oceans play a major role for the circulation in the Nordic Seas and the Atlantic (and possibly the World) Ocean since it passes convective regimes of major importance to the thermohaline circulation (Aagaard and Carmack 1989). The role of high latitude freshwater input is of particular interest from a paleo perspective. The response of the ocean circulation to increased melt water fluxes during the last deglaciation (14-15 kyr BP) can possibly explain the highly variable climate during this period (e.g., Broecker et al. 1992; Lehman and Keigwin 1992; Clark et al. 2002).

Simonsen (1996) computed the melt water fluxes into the Atlantic Ocean, the Nordic Seas and the Arctic Ocean based on the paleo-topography reconstruction of Peltier (1994). The obtained 1000 years mean melt water flux into the Nordic Seas and the Arctic Ocean was comparable with the modern freshwater input of 0.1 Sv (1 Sv = 10^6 m^3 s^{-1}; Aagaard and Carmack 1989) during the last deglaciation. However, paleo data records indicate that the major melting lasted only 300-500 years (Fairbanks 1989; Jones and Keigwin 1988), implying freshwater fluxes 2-3 times larger than the 1000 year mean during the major melting events.

Fully coupled atmosphere-sea ice-ocean climate models are currently used to examine the past, present and possibly future climate states. The present day climate models give a fairly representative picture of several aspects of the current climate system (e.g., Latif 1998; Cooper and Gordon 2002; Furevik et al. 2003). Many state-of-art climate models show a 20-30 % reduction in the Atlantic Meridional Overturning Circulation (AMOC) when forced with greenhouse gas and aerosol projections for the current century (e.g., Cubasch et al. 2001).

A typical and quite robust response in coupled model simulations is increased evaporation at low latitudes, and increased precipitation and continental runoff to the high northern latitudes. It is therefore tempting to believe that increased supply of freshwater and warming at high northern latitudes will lead to reduced formation rates of intermediate and deep water masses, and consequently to a reduced AMOC (Peterson et al. 2002). However, a different model response was identified by Latif et al. (2000). Here, large-scale air-sea interactions in the tropics, with a pattern similar to a strong and persistent El Niño (Timmermann et al. 1998), lead to anomalously high salinities in the tropical Atlantic. These anomalies were then advected northward into the convective regions of the North Atlantic, and thereby compensating for the effect of local warming and freshening. Also other model experiments show essentially no changes in the AMOC during the 21st century (Gent 2001; Sun and Bleck 2001).

In addition to increased freshwater fluxes at the high northern latitudes, most climate models show an enhanced greenhouse warming in the polar regions, especially for the Arctic, with a predicted warming of 3-4°C during the next 50 years (Mitchell et al. 1995; Räisänen 2001). This will most likely lead to changes in both the extent and the thickness of sea ice in the Arctic, with consequences for the Arctic region (Vinnikov et al. 1999; Johannessen and Miles 2000).

In this report we address these questions by exploring the isolated effects of increased freshwater input to the Arctic Ocean and Arctic warming, the latter manifested as a gradually reduction in the sea ice thickness, by means of idealized model experiments. For the experiments, an isopycnic coordinate OGCM fully coupled to a dynamic-thermodynamic sea ice model has been used (see Sec. 2). The model experiments are described in Sec. 3, and the results of the control and perturbed simulations are provided in Secs. 4 and 5, respectively. The obtained results are discussed in Sec. 6, and the findings are summarized in Sec. 7.

2 The coupled ocean - sea ice model

The OGCM applied in this study is based on the Miami Isopycnic Coordinate Ocean Model (MICOM) (see Bleck et al. 1992 for a thorough description of the model). To describe the high latitude climate system, dynamic and thermodynamic sea ice modules have been coupled to MICOM (Drange and Simonsen 1996). The sea ice module modifies the heat and freshwater fluxes between the ocean and the atmosphere by freezing or melting ice in order to prevent the sea surface temperature to decrease below the freezing point of sea water T_f (°C). If ice is present and the sea surface temperature increases, ice is melted in order to keep the sea surface temperature at the freezing point. The dynamic ice model, which transports ice as a result of the applied wind field and the simulated surface currents and sea surface tilt, is based on the classical viscous-plastic rheology of Hibler (1979), but in the modified implementation of Harder (1996).

For this study a regional version of MICOM has been adopted. The model domain includes the Atlantic Ocean north of 20°S and the entire Arctic Basin (Fig. 1). A locally orthogonal curvilinear horizontal grid (Simonsen and Drange 1997) was adopted with grid focus in the Nordic Seas with a maximum grid resolution of about 40 km. Artificial (closed) boundaries occur south of the Bering Strait, along the South Atlantic boundary and in the Strait of Gibraltar.

The model was initialized with temperature and salinity fields for September from the National Oceanographic Data Center (Levitus et al. 1994; Levitus and Boyer 1994), and is forced by monthly mean climatologic atmospheric fields. The wind stress and absolute wind speed were derived from the European Centre for Medium Range Weather Forecasts (ECMWF 1988), merged with data from the Comprehensive Ocean Atmosphere Data Set (COADS) in the central Atlantic Ocean (Oberhuber 1988; Aukrust and Oberhuber 1995). Cloud cover and relative humidity are from COADS, with data from Huschke (1969) and Maykut (1978) included in the central Arctic, respectively. The air temperature is from the COADS data set, but with data from ECMWF and coastal weather stations in ice covered regions as prepared by Simonsen and Haugan (1996). Precipitation is derived from Legates and Willmott (1990).

The major rivers in the model domain are included. The seasonal variation in the river output is adopted from Dümenil et al. (1993). For those rivers where the seasonal variation is unknown, the variation from a neighbouring river is used. The annual mean river discharge is adopted from Aagaard and Carmack (1989), Dümenil et al. (1993), Mosby (1962) and Semtner (1987), and amounts to about 0.1 Sv for the Arctic rivers (the location of the major Arctic rivers are indicated in Fig. 1). A virtual salt flux formulation is used for the river runoff in the model (fixed ocean volume and no volume flux). Therefore, no additional mass of water is added through river runoff. Since the virtual salt flux formulation cannot conserve the ocean salt content (Roullet and Madec 2000), a restored sea surface salinity (SSS) is used to limit the surface salinity drift.

The model was first spun up for 40 years. This is too short to draw any definite conclusions about the model performance. However, at this point an annual steady state circulation was achieved, and the main features of the circulation in the Arctic Ocean, the Nordic Seas were reproduced. During the spin-up, relaxation of sea surface temperature (SST; Levitus and Boyer 1994) and SSS (Levitus et al. 1994) was applied. Since there are few hydrographic observations from the Arctic, relaxation of SST was switched off wherever the monthly sea ice climatology by Walsh and Johnson (1979) showed ice, whereas relaxation of SSS was made towards the annual mean salinity field of the area. After the spin up period of 40 years, the model was run for another three years with continued relaxation applied to temperature and salinity. During this period, the salt flux implied by the SSS relaxation was diagnosed and monthly mean values were computed and stored.

A total of three 50 years long simulations were then carried out (see below). During the three

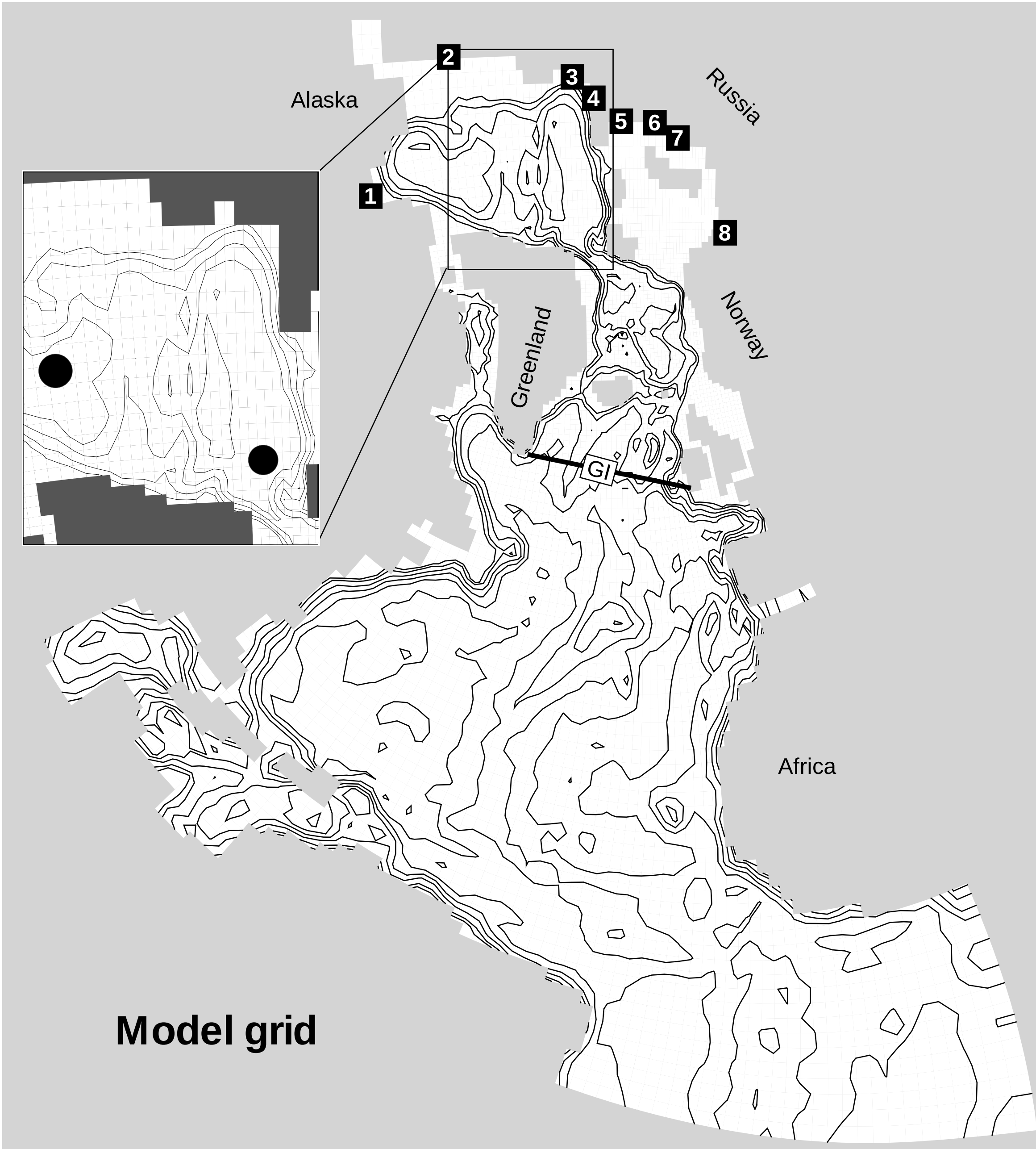

Figure 1: The model grid used in this study. The numbers 1–8 represent the major river discharge locations in the Arctic Ocean (MacKenzie, Kolyma, Kotuy, Lena, Ob, Yenisei, Pyasina and Northern Dvina, respectively). Also shown are two locations in the Arctic Ocean, one in the Eurasian Basin and a second one in the Canadian Basin. Finally, the Greenland-Ireland transect used in the text is shown.

model experiments, the diagnosed monthly mean SSS flux was applied for the SSS relaxation in order to let SSS anomalies freely develop, propagate and decay in the model, while SST relaxation was activated.

3 Design of the freshwater experiments

All of the 19 climate models participating in the Coupled Models Intercomparison Project CMIP-2 predict increased precipitation and enhanced warming in the high northern latitudes in response to increased greenhouse gas forcing (Räisänen 2001). The magnitude of the increase in precipitation depends on the model (Räisänen 2001), and likely on the strength of the applied greenhouse gas forcing. For instance, in the transient greenhouse warming simulation by Latif et al. (2000), an increased freshwater flux (precipitation minus evaporation plus river runoff) of 0.1 Sv was found poleward of 45°. Furthermore, Manabe and Stouffer (1994) obtained an increased freshwater flux of 0.3 Sv poleward of 50°N in a global warming scenario assuming a 1 % increase in the concentration of atmospheric CO_2 until a quadrupling of the present value was reached. If the simulated changes in the freshwater fluxes are confined to the Arctic Ocean and the Barents Sea, a doubling to tripling of the present river runoff of about 0.1 Sv (Aagaard and Carmack 1989) is obtained.

Based on the scenario-derived estimates of increased freshwater flux to the high northern latitudes, idealized model experiments with a doubling and a fivefold increase (for comparison) of the freshwater fluxes to the Arctic region have been conducted. Together with the increased freshwater fluxes, the thickness of the Arctic sea ice have been reduced to mimic an expected sea ice response to global warming (Vinnikov et al. 1999, see Sec. 3.1). The three integrations are

CTRL: No change in the freshwater flux.

PX2: Doubling of the freshwater fluxes from the Arctic rivers plus reduced sea ice thickness.

PX5: Fivefold increase in the freshwater fluxes from the Arctic rivers plus reduced sea ice thickness.

3.1 Artificially reduced sea ice thickness

Fresh water added to seawater changes the thermodynamic properties of seawater in several ways. If one considers a well mixed surface layer of thickness h_{ml} (m) with temperature T_{ml} (°C) and salinity S_{ml} (psu), the mixed layer temperature and salinity will be modified according to the volumetric expressions

$$S^*_{\mathrm{ml}} = \frac{h_{\mathrm{ml}}}{h_{\mathrm{ml}}+\delta} S_{\mathrm{ml}} \quad \text{and} \quad T^*_{\mathrm{ml}} = \frac{h_{\mathrm{ml}}\, T_{\mathrm{ml}} + \delta\, T_{\mathrm{fw}}}{h_{\mathrm{ml}}+\delta}$$

upon addition of δ (m) freshwater with temperature T_{fw} (°C) and vanishing salinity. For simplicity, the different heat capacities and densities of freshwater and seawater have been ignored in the expression of T^*_{ml}.

Through most of the year, $T_{\mathrm{fw}} > T_{\mathrm{ml}}$ in sea ice covered regions. Therefore, the surface salinity decreases and the surface temperature increases as freshwater is added to the system. It is not given how the modified surface salinity and temperature may influence the growth rate of sea ice since T_f depends on salinity (Millero 1978), and since the difference between T_{fw} and T_{ml} is one of the factors that determine the growth rate of sea ice (Drange and Simonsen 1996).

The modified freezing point of seawater T^*_f can be approximated by the expression

$$T^*_{\mathrm{f}} = 0.066 - 0.057\, S^*_{\mathrm{ml}}$$

for salinities in the range 30–36 psu (Drange and Simonsen 1996). Since $\delta \ll h_{\mathrm{ml}}$, it follows from $\partial S^*_{\mathrm{ml}}/\partial\delta$ and $\partial T^*_{\mathrm{ml}}/\partial\delta$ that

$$\frac{\partial T^*_{\mathrm{ml}}}{\partial S^*_{\mathrm{ml}}} = \frac{T_{\mathrm{ml}} - T_{\mathrm{fw}}}{S_{\mathrm{ml}}}.$$

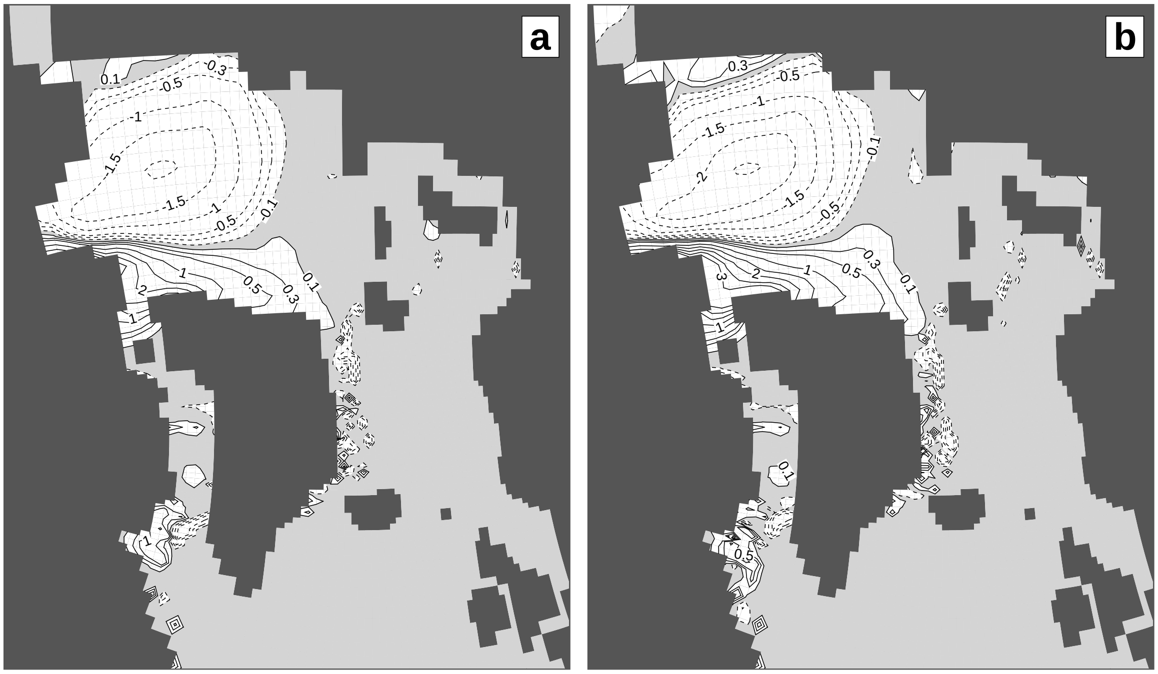

Figure 2: Difference in sea ice thickness (m) compared to CTRL for (a) PX2 and (b) PX5. Dotted lines represent reduced sea ice thickness. Contour interval (CI) is 0.5 m. In addition the ±0.3 m and ±0.1 m contour levels are shown.

In polar regions, the temperature difference $T_{\mathrm{fw}} - T_{\mathrm{ml}}$ is typically a few °C, and for a surface salinity in the range 30–36 psu, we get that

$$\frac{\partial T^*_{\mathrm{ml}}}{\partial S^*_{\mathrm{ml}}} \approx -0.06 \text{ and } \frac{\partial \mathrm{T}^*_{\mathrm{f}}}{\partial \mathrm{S}^*_{\mathrm{ml}}} = -0.057.$$

Therefore, as a first approximation, the supply of freshwater to ice covered seawater leads to a change in the surface temperature given by $\partial T^*_{\mathrm{ml}} \approx \partial T^*_{\mathrm{f}}$. The consequences of these considerations are that the supply of freshwater through S^*_{ml} and T^*_{ml} will not, as a first approximation and from a purely thermodynamic point of view, change the growth rate (i.e., thickness) of sea ice despite $T_{\mathrm{fw}} > T_{\mathrm{ml}}$.

In this study, it is assumed that the Arctic warming vary in accordance with the applied freshwater fluxes. Furthermore, an *ad hoc* assumption is made that the warming corresponds to the change in T^*_{ml}, i.e., to the change in the mixed layer temperature caused by the added freshwater. This assumption leads to a reduced sea ice thickness of 1.5–2 m in the central Arctic (Fig. 2). The obtained melting rates correspond to those found in scenario integrations with fully coupled climate models (Vinnikov et al. 1999), indicating that the applied melting rate of sea ice is reasonable compared to fully coupled climate models.

4 The CTRL simulation

Time series of the annual averaged SSS and SST over the entire model domain over the 50 year integration period show relatively small drifts in SSS (0.03 psu) and SST (0.08 °C; Fig. 3). The

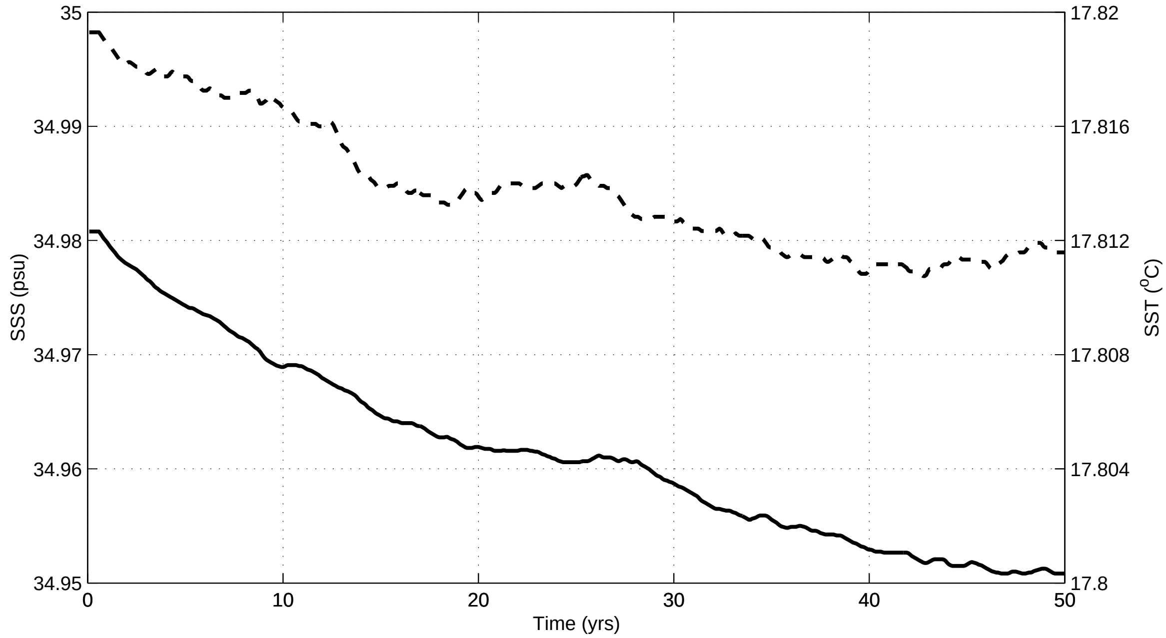

Figure 3: Time series of the annual mean sea surface salinity (psu; solid line) and sea surface temperature (°C; dashed line) for the model domain in CTRL.

volume transports through some key passages in the model also remain fairly stable (Fig. 4). However, a reduction in the transports across the Greenland-Ireland (GI) section can be noted, as well as a slight increase in the transport over the Faroe-Shetland Channel (FSC). This could indicate a slight rearrangement of the splitting of the NAD south of Iceland, with relatively more AW entering the FSC rather than the subpolar gyre. In the Arctic Ocean, the volume transports across the Fram Strait is stable throughout the integration period.

It should be noted that a changed climate system will, in general, lead to changes in all of the air-sea ice-sea fluxes. The presented perturbation integrations should therefore be viewed as idealized sensitivity experiments only.

It should be mentioned that the new equilibrium states will only be reached after several thousand years of integration time. Important transitions in circulation can occur after more than 50 years (Rahmstorf 1995), even if SST and SSS drifts are slow. An integration period of 50 years is therefore too short to draw any firm conclusions on the model performance. With this shortcoming in mind, CTRL is discussed based on the first year of the (CTRL) simulation.

4.1 The Arctic Ocean and the Barents Sea

In the Arctic Ocean, two main features characterize the surface currents (Carmack 1990). The first is the Transpolar Drift (TD), in which the surface waters of the Eurasian Basin move across the basin towards the North Pole and then towards the Fram Strait. The second is an anticlockwise flow in the Canadian Basin, the so-called Beaufort Gyre (BG). While the BG seem to be well reproduced by the model, the TD is directed towards the northern part of Greenland rather than the Fram Strait (Fig. 5).

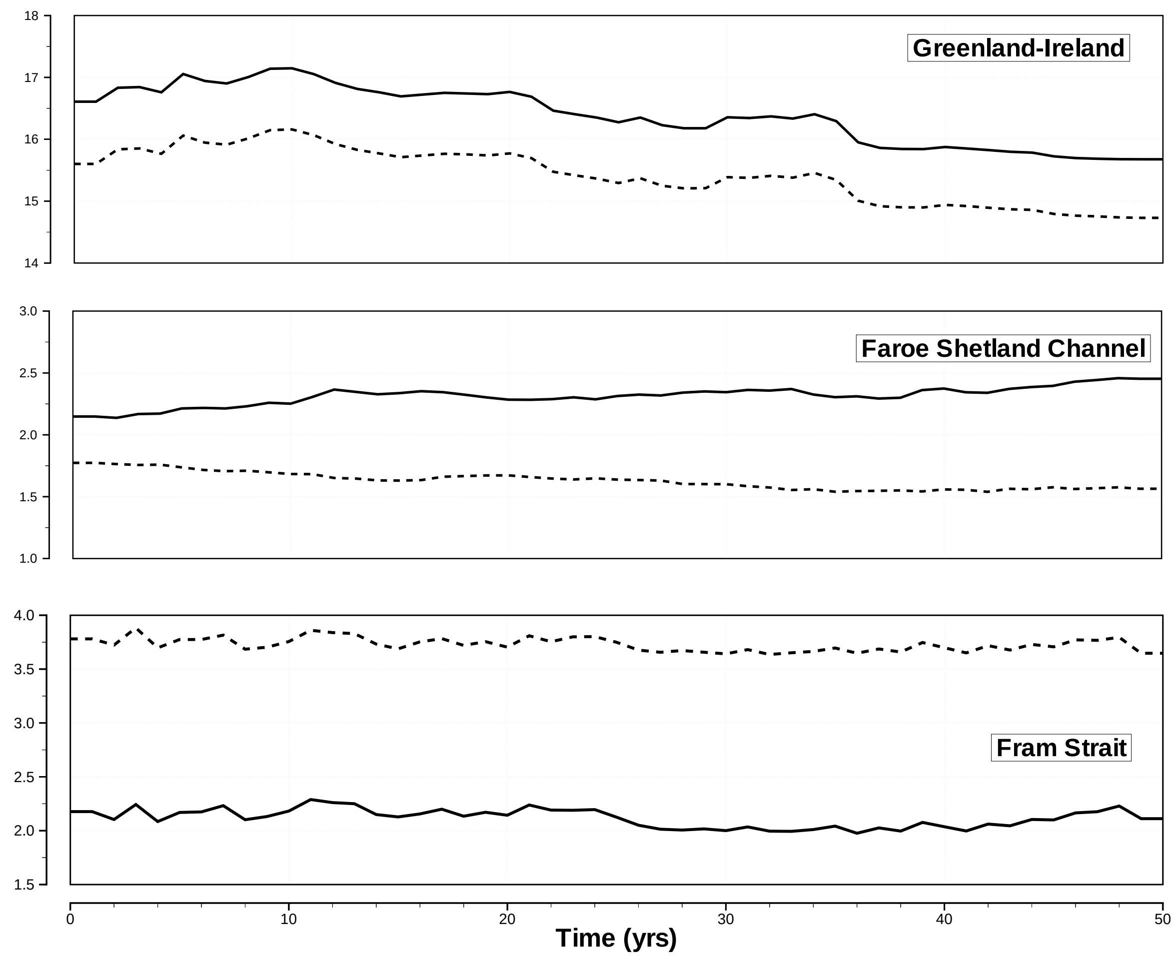

Figure 4: Time series of the net annual mean northward (solid line) and southward volume transports (Sv) for the GI section, the FSC and the Fram Strait in CTRL.

The upper waters of the Arctic Ocean are characterized by a shallow mixed layer at or near the freezing point, overlying a pronounced cold halocline (Rudels et al. 1996). The halocline is a layer with temperatures $< -1°$C and salinities between 30.4-34.4 psu, leading to a stable vertical density structure in the central Arctic. The model capture a halocline at a depth of about 100-200 m which agree quite well with observations (Fig. 6).

However, the Atlantic layer is not well reproduced in the model (Fig. 6). For instance, the water at intermediate depths in the Eurasian Basin is too cold (by about 1°C) compared to observations taken during the *Oden* 91 expedition (Anderson et al. 1994). The reason for this is not yet clear, but it could be linked to a too intense cooling, and consequently to a too vigorous surface mixing in the West Spitsbergen Current south of the Fram Strait in the model.

The model is able to generate ice cover in fairly good agreement with climatologies derived from observations (Johannessen et al. 1999). In winter, the ice covers all of the Arctic Ocean, the Kara Sea and the western part of the Barents Sea (Fig. 7a). The maximum sea ice thickness occurs north of

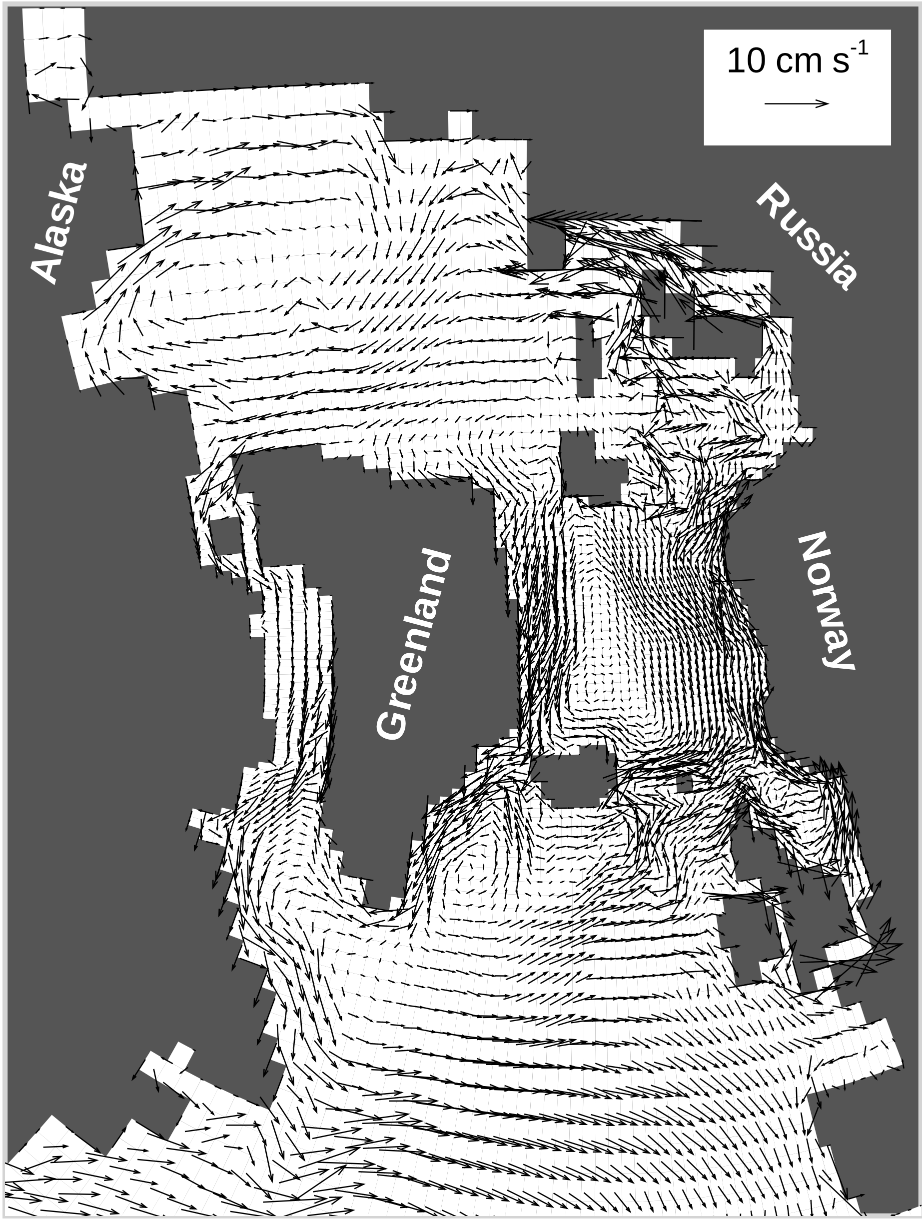

Figure 5: Simulated annual mean sea surface velocity field (cm s^{-1}) at the start of CTRL.

Greenland and the CA, and is in agreement with other studies (e.g., Kreyscher et al. 2000). The sea ice velocity shows a clockwise circulation over the Canadian Basin, and the TD is evident over the Eurasian Basin (Fig. 7b). There is also a drift towards northwestern Greenland and the CA, leading to the accumulation of ice there.

The exchange of water masses between the Arctic Ocean and the North Atlantic in the model takes place through three passages, the CA, the Fram Strait and the Barents Opening. The model, as adapted for this study, ignores the inflow of mass and momentum from the Bering Strait, which amounts to

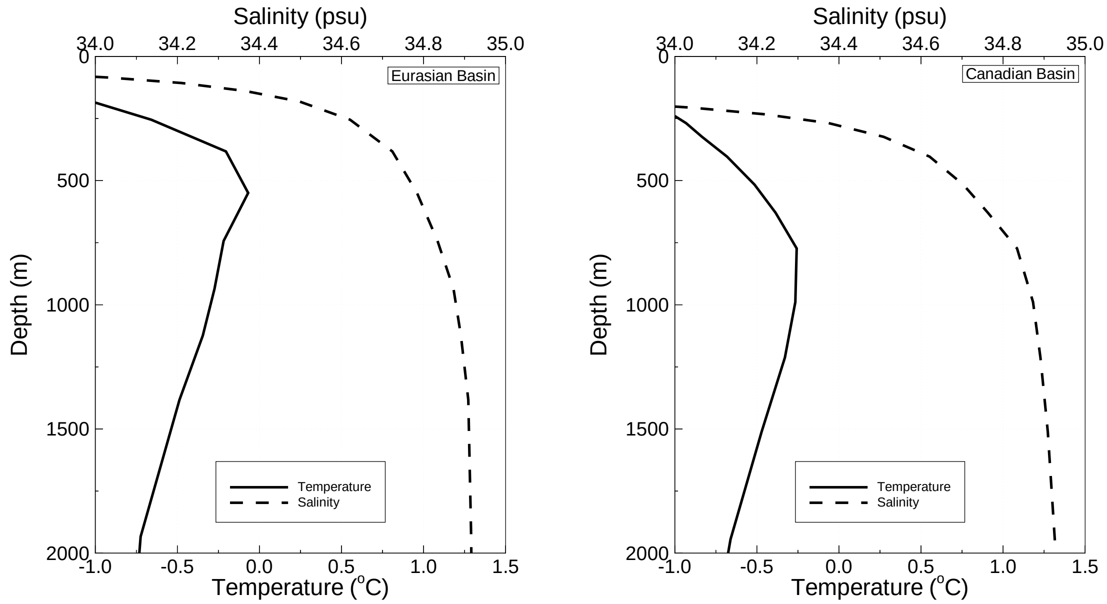

Figure 6: Modelled vertical temperature and salinity profiles for the Eurasian Basin (left panel) and the Canadian Basin (right panel) (see Fig. 1 for location).

about 0.8 Sv based on observations (Roach et al. 1995). The Pacific water carried northwards through this passage is important, since this water ventilates the Arctic Ocean halocline (Roach et al. 1995), with potential consequences for the circulation and sea ice cover in the Arctic Ocean. However, relaxation towards observed annual mean salinity results in realistic sea surface salinity fields for the Bering Strait.

In the model, there is a southward transport of about 1.2 Sv through the CA and of about 1.6 Sv through the Fram Strait (Fig. 8). These fluxes are compensated by a net inflow through the Barents Opening of about 2.8 Sv, yielding a balance of mass for the Arctic Ocean. The obtained water fluxes are in general agreement with observational based estimates (Simonsen and Haugan 1996). Some seasonal variation can be seen in the transports through the Fram Strait and the Barents Opening, but not so much in the outflow through the CA.

4.2 The Nordic Seas and the northern North Atlantic

The model describe the major current systems in the Nordic Seas and the north Atlantic Ocean (Fig. 5). In the Nordic Seas, two major currents characterize the circulation. These are the Norwegian Atlantic Current (NwAC) in the east, and the East Greenland Current (EGC) in the west, both of which are captured by the model. In addition, a zonal, eastward flow between the EGC and the NwAC can be seen northeast of Iceland, often referred to as the East Iceland Current. All of these currents describe a large cyclonic circulation pattern in the Nordic Seas. In the Labrador Sea, a relatively strong Labrador Current can be seen to flow southward towards Newfoundland. In the Irminger Basin, a branch of the NAD, the Irminger Current, flows north towards the Denmark Strait where most of it is captured by the strong EGC, thus forming a cyclonic circulation pattern in this area.

Warm and saline AW (T of $\sim$9-10°C and S of about $\sim$35.1 psu) can be seen to enter the Nordic

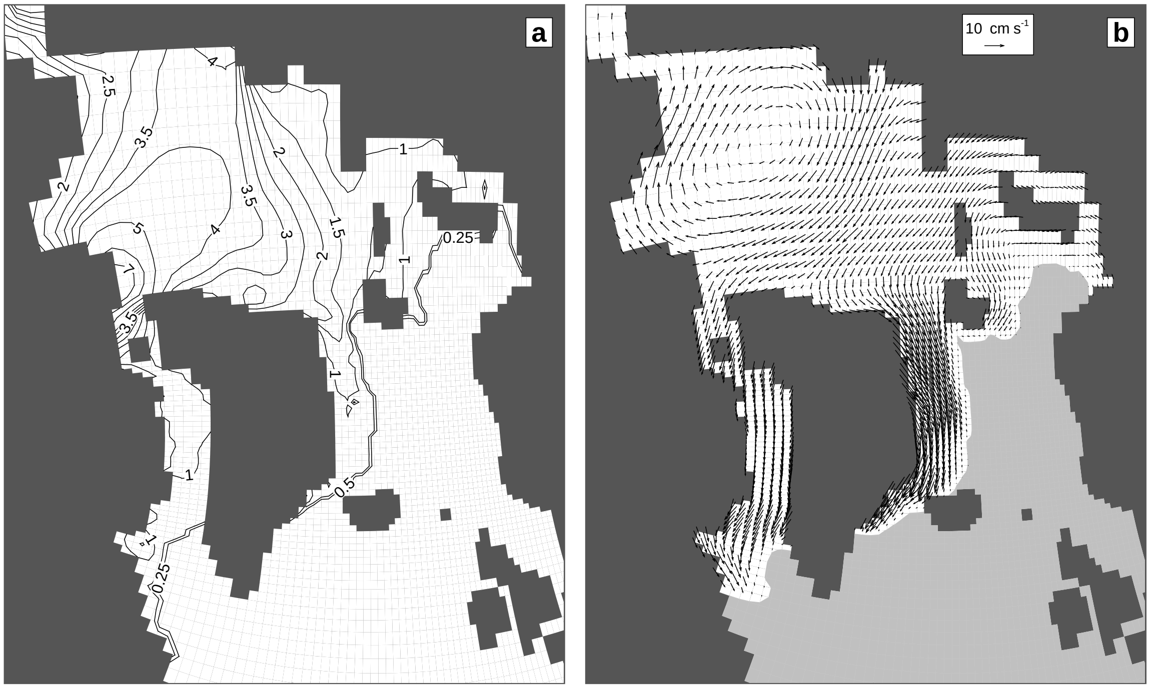

Figure 7: (a) Sea ice thickness (m; left panel) in March at the start of CTRL, and (b) annual mean sea ice velocity (cm s^{-1}) in the first year of CTRL. In panel (a), CI is 0.5 m. In addition the 0.25 m contour level is shown.

Seas north of Scotland through the FSC (Fig. 9a,b). On its way northwards the water cooles yielding relatively deep mixed layers in the Greenland, Irminger and Labrador Seas in winter (Fig. 9c). The model is therefore at least qualitatively able to reproduce the formation of subsurface water masses in these regions. However, in the Labrador Sea, the model seems to underestimate the mixed layer thickness (only about 600 m).

The model produces an inflow of AW over the Iceland-Faroe Ridge (IFR) of about 2.6 Sv (Fig. 8). This is in good agreement with an estimate of 2.9 Sv for the Faroe Current based on current measurements (Hansen et al. 1998), but 1.1 Sv below an estimate reported for the IFR in Hansen and Østerhus (2000). Estimates of the deep overflow through the FSC vary between 1.1–1.9 Sv in literature (Simonsen and Haugan 1996). The model obtains an intermediate and deep overflow of about 1.8 Sv, which is inside this range. The model obtains a total inflow to the Norwegian Sea across the FSC of about 2.2 Sv in the surface and intermediate layers (Fig. 8), which is somewhat lower than expected from the most recent observations (Hansen and Østerhus 2000).

In the Denmark Strait, there is a total southward volume transport of about 2.1 Sv (Fig. 8). Of this, about 0.9 Sv is due to transport in the intermediate and deep layers, while the export with the EGC in the surface is about 1.2 Sv. These estimates are lower than expected from literature where transport estimates of 3 Sv are found for both the EGC and the deep overflow (Hopkins 1991). A too coarse grid resolution may be one of the reasons for this.

Despite the commented model deficiencies, CTRL reproduces most of the major features of the modern ocean circulation in the North Atlantic, the Nordic Seas and the Arctic Ocean, and should therefore provide a fairly realistic framework for the perturbation experiments.

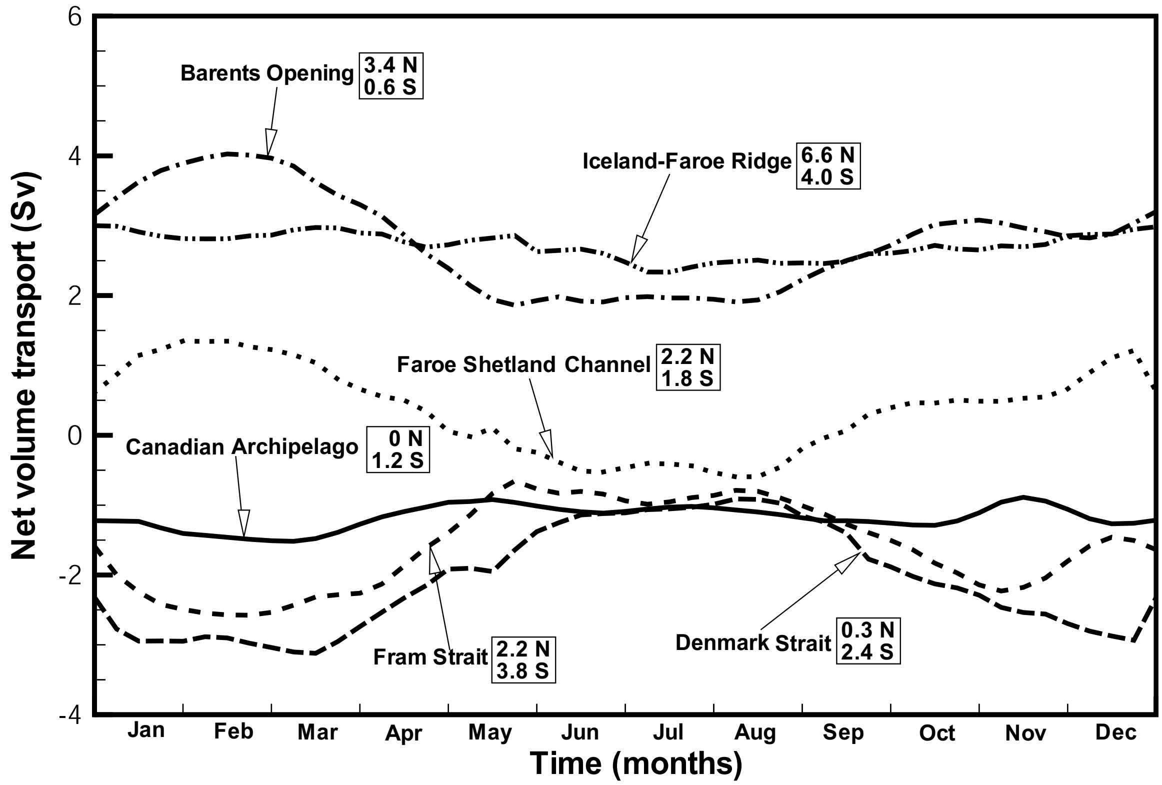

Figure 8: Total transports of mass the major passages in the Nordic Seas and the Arctic Ocean at the start of CTRL. (a) Volume transport (Sv) and (b) heat transport (TW). The annual mean northward (N) and southward (S) volume transports are also shown.

5 The perturbed simulations

5.1 The Arctic Ocean

In the Arctic, the major differences in SSS in the freshwater simulations are found downstream of the river discharge areas in Canada, Siberia and Russia, and after 50 years all of the Arctic Ocean is influenced (Fig. 10). Off the Siberian coast, a clear freshwater belt follows the TD towards Greenland. A large part of this flow enters the Canadian Basin, where it accumulates in the BG.

Because of the increased freshwater input, a strong density gradient is set up along the periphery of the central Arctic Ocean (Fig. 11). This in turn influences the horizontal pressure gradients, and by that the mixed layer flow. Over the Canadian Basin the sea surface height increases by 40 cm and 60 cm in PX2 and PX5, respectively (Fig. 12). The pressure gradients associated with the sea surface elevation lead to the surface geostrophic flow components u_s and v_s (m s^{-1}) described by

$$u_s = -\frac{g}{f}\frac{\partial \zeta}{\partial y}, \text{ and } v_s = \frac{g}{f}\frac{\partial \zeta}{\partial x}.$$

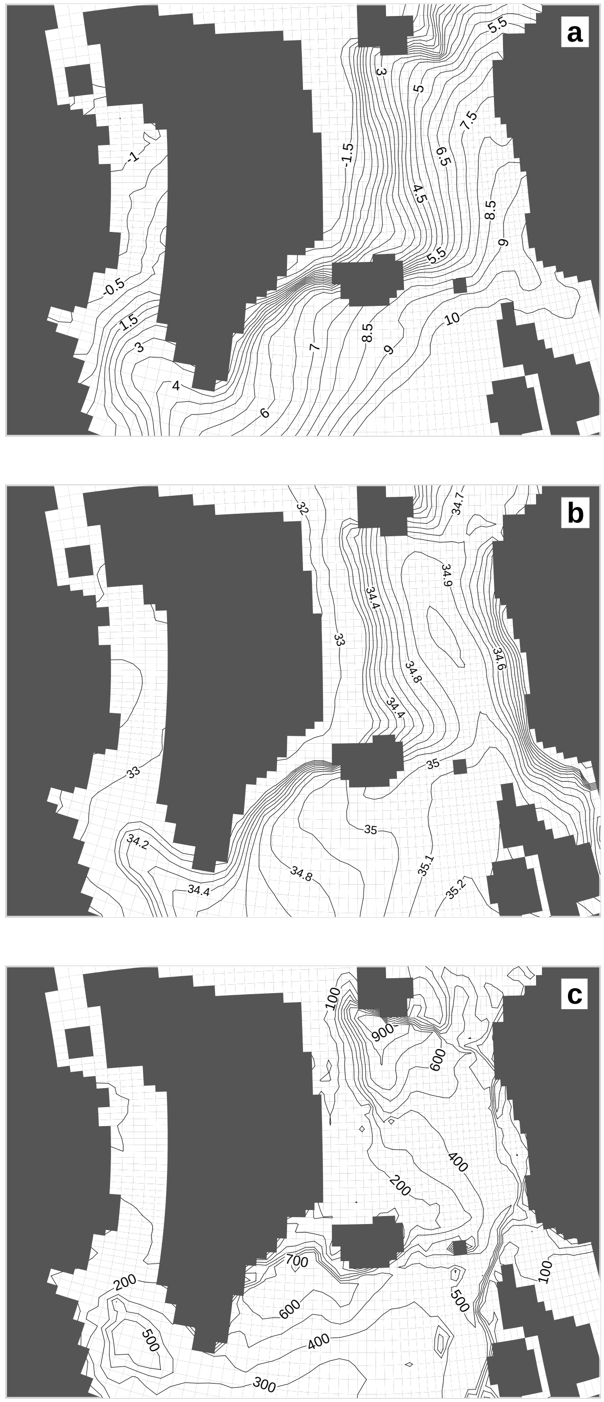

Figure 9: Mixed layer properties for the Nordic Seas and the northern North Atlantic at the start of CTRL. (a) Annual mean sea surface temperature (°C), (b) annual mean sea surface salinity (psu) and (c) winter mixed layer thickness (m). CIs are (a) 0.5°C, (b) 0.1 psu for contour values ≥34, and (c) 100 m. In (b) the 32 and 33 psu contour levels are also shown.

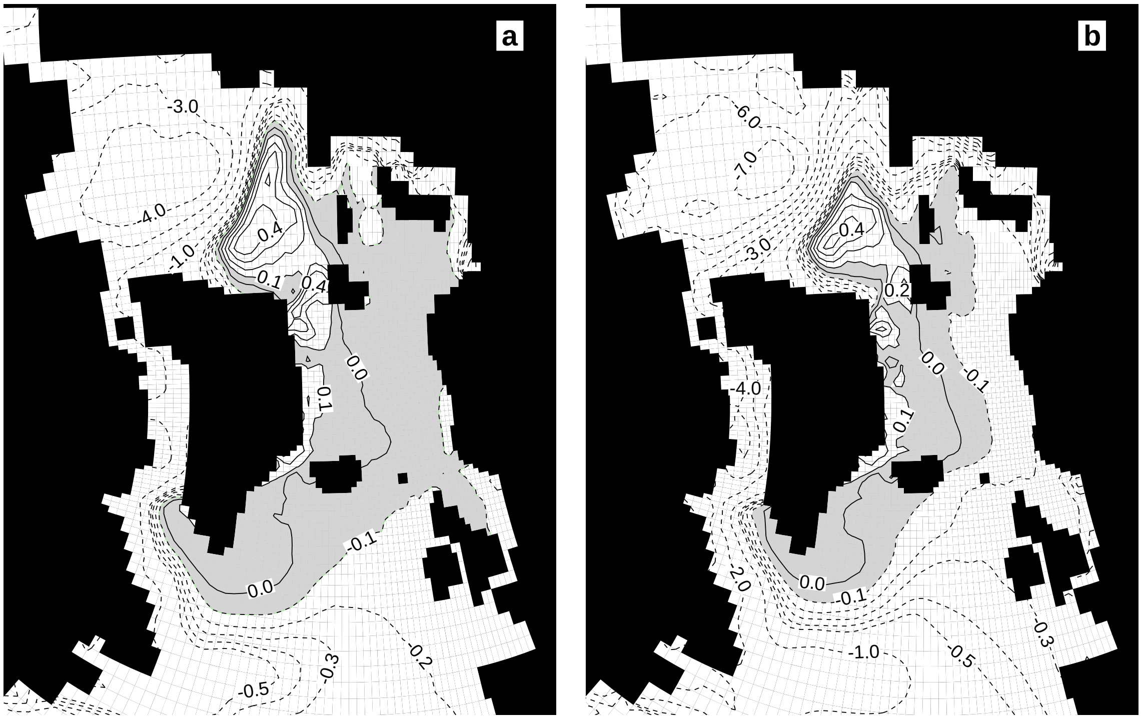

Figure 10: Difference in annual mean sea surface salinity compared to CTRL in year 50. (a) PX2, and (b) PX5. Dotted lines represent negative anomalies. CI is 1 psu. In addition the contour lines from -0.5 to 0.5 psu are shown in CI of 0.1 psu.

Here g (m s^{-2}) is gravity, f (s^{-1}) is the Coriolis parameter, and ζ (m) is the height of the surface above a reference level. A relatively strong increase in the currents (about 5 cm s^{-1} in the PX5 simulation) is found in the Beaufort Gyre, leading to an intensified drift towards the CA (Fig. 13). The changes in the Eurasian Basin are smaller, with the only significant change being an increased drift towards the Laptev Sea in the northern part of the Eurasian Basin.

Furthermore, the artificially reduced sea ice thickness of between 1.5–2 m in the central Arctic Ocean also has an impact on the sea ice velocity field (Fig. 14). An increase of about 3-5 cm s^{-1} is found in the BG. This change is partly attributed to the intensified geostrophic flow (Fig. 13), and partly to the increased momentum transfer through the thinner sea ice.

The simulated change in the sea surface flow field is given in Fig. 15. In PX5, an increase in excess of 6 cm s^{-1} is found in the BG. The major part of this change (about 80 %) is caused by changes in the geostrophic currents (Fig. 13), while the rest is caused by the reduced sea ice thickness and by that the increased sea ice velocity. A consequence of the changes in the circulation in the Arctic is a gradual increase in the net southward transport through the CA throughout the whole integration period, reaching almost 0.3 Sv and 0.5 Sv in year 50 in PX2 and PX5, respectively (Fig. 16). The increase in the southward transport is compensated further east through the Fram Strait where the net southward transport is reduced and through the Barents Opening where an increase in the net northward transport is obtained during the last part of the integration (not shown).

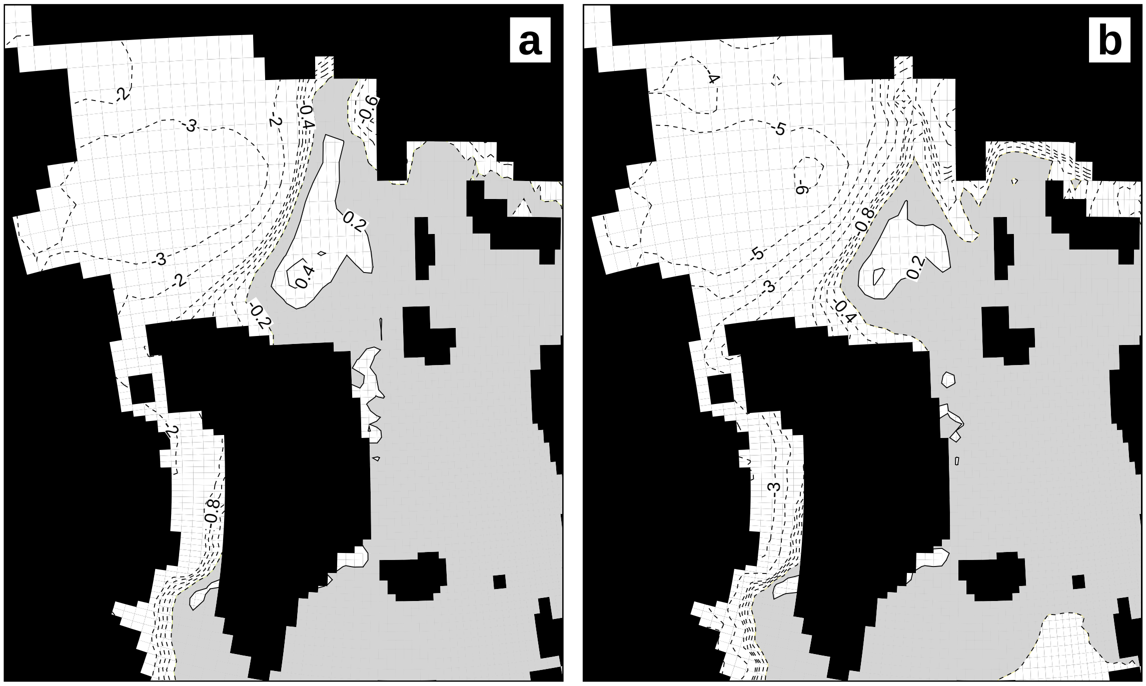

Figure 11: Difference in the mixed layer density (in σ_0-units) between CTRL and the perturbed simulations. (a) PX2 and (b) PX5. CI is 0.2 between -1 and 1, and 1 elsewhere. Negative values indicate reduced density.

5.2 The Nordic Seas and the northern North Atlantic

The net northward transport of AW across the GI section (see Fig. 1) increases gradually, reaching about 0.3 Sv and 0.5 Sv for PX2 and PX5, respectively (Fig. 17). The increased northward transport thus compensates for the increased southward transport of mass through the Canadian Archipelago.

Most of the change in the northward transport of AW entering the Nordic Seas takes plase in the FSC, where an increase in the net northward mass transport reach 0.2 Sv and 0.4 Sv in PX2 and PX5, respectively (Fig. 17). As a consequence of this, there is an increase in the supply of both heat and salt to the Nordic Seas through this passage (Figs. 18 and 19). The changes in the transports across the IFR are similar, but smaller than those in the FSC. In the Denmark Strait, only minor changes are found in the net volume transport in PX2, while an increased southward transport in excess of 0.2 Sv is seen in PX5.

The simulated mixed layer thickness is the best measure of the formation of sub-surface and abyssal waters in the model. The strongest response to the enhanced freshwater input is found in the Labrador Sea (Fig. 20). The initial response is a rapid decrease in the mixed layer thickness of 110 m and 180 m in PX2 and PX5, respectively (Fig. 20a). However, from year 10 and onwards a gradual recovery can be seen, leading to an almost complete recovery of the mixed layer in year 50. In the Irminger Sea, the response is much weaker, with a maximum reduction around year 30 of about 40 m and 60 m in PX2 and PX5, respectively, and a slight increase in the ML thickness at the end of the integration (Fig. 20b). In the Greenland Sea, a rapid reduction in the mixed layer thickness of about 30 m and 70 m can be seen between years 10-20 in PX2 and PX5, respectively (Fig. 20c). However,

Figure 12: Difference in sea surface height (cm) between CTRL and the perturbed simulations. (a) PX2 and (b) PX5. CI is 2 cm between -10 to 10, and 10 cm elsewhere.

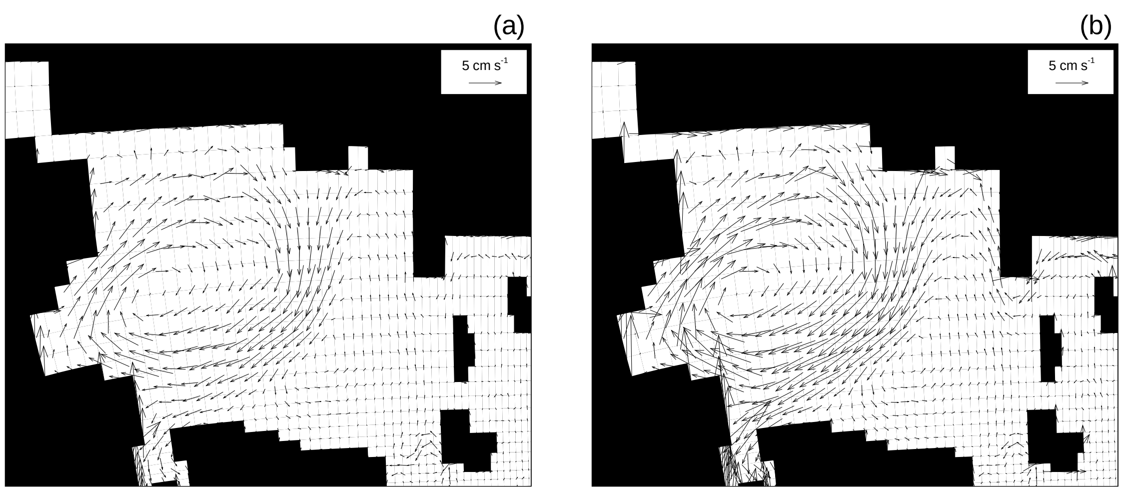

Figure 13: Difference compared to CTRL in the annual mean geostrophic surface current (cm s^{-1}) in year 50 for (a) PX2 and (b) PX5.

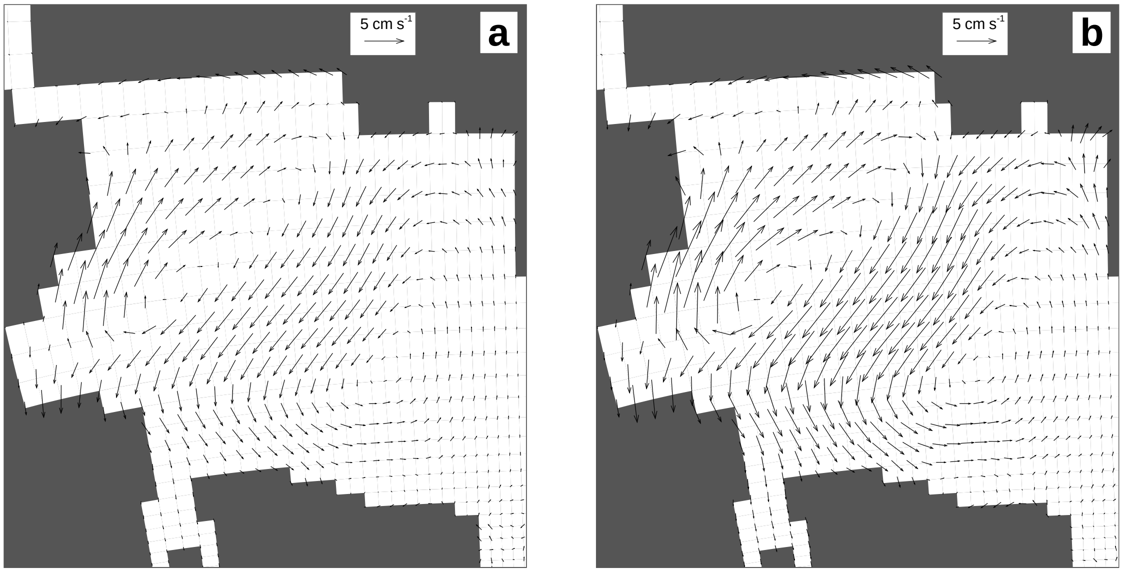

Figure 14: Difference compared to CTRL in the annual mean sea ice velocity (cm s^{-1}) in year 50 for (a) PX2 and (b) PX5.

for the rest of the period the mixed layer thickness remains relatively stable.

The reason for the recovery and stabilization of the mixed layer thickness in the Labrador and Greenland Seas are the increased northward transport of AW with the NAD (Figs. 15 and 17). As a result of the intensified NAD, more salt are transported into these regions (Fig. 19), increasing the density, and by that compensating for the enhanced freshwater input from the Arctic.

6 Discussion

The obtained model response indicates that the combined effect of increased freshwater supply to the Arctic Ocean and reduced sea ice thickness tend to have a near stabilizing effect on the NAD. Firstly, the increased freshwater released in the Arctic Ocean leads to a stabilization of the water column in the Atlantic sub-polar gyre and in the Nordic Seas, resulting in a weakened NAD. Secondly, intensified geostrophic currents due to increased density gradients in the central Arctic Ocean and more efficient transfer of momentum through the thinner sea ice lead to an intensified BG. A consequence of these changes is that the southward transport of mass through the CA increases. Since the Arctic Ocean, the Barents Sea and the Nordic Seas constitute a closed system (assuming that the flow through the Bering Strait remains fairly constant), this loss of water has to be replaced. In the model, this is accomplished through an intensified NAD, resulting in an ocean state found in CTRL.

Since the flow through the Bering Strait is governed by the difference in the sea level height (SLH) across the strait, it is expected that the flow of Pacific water into the Arctic Ocean will decrease as a consequence of the change in SLH in the freshwater experiments. Therefore, an open Bering Strait with reduced poleward volume flow will also tend to strengthen the NAD.

Typical climate model responses to global warming scenarios are increased evaporation at low latitudes and increased precipitation, runoff and glacial melting at high latitudes (Manabe and Stouffer

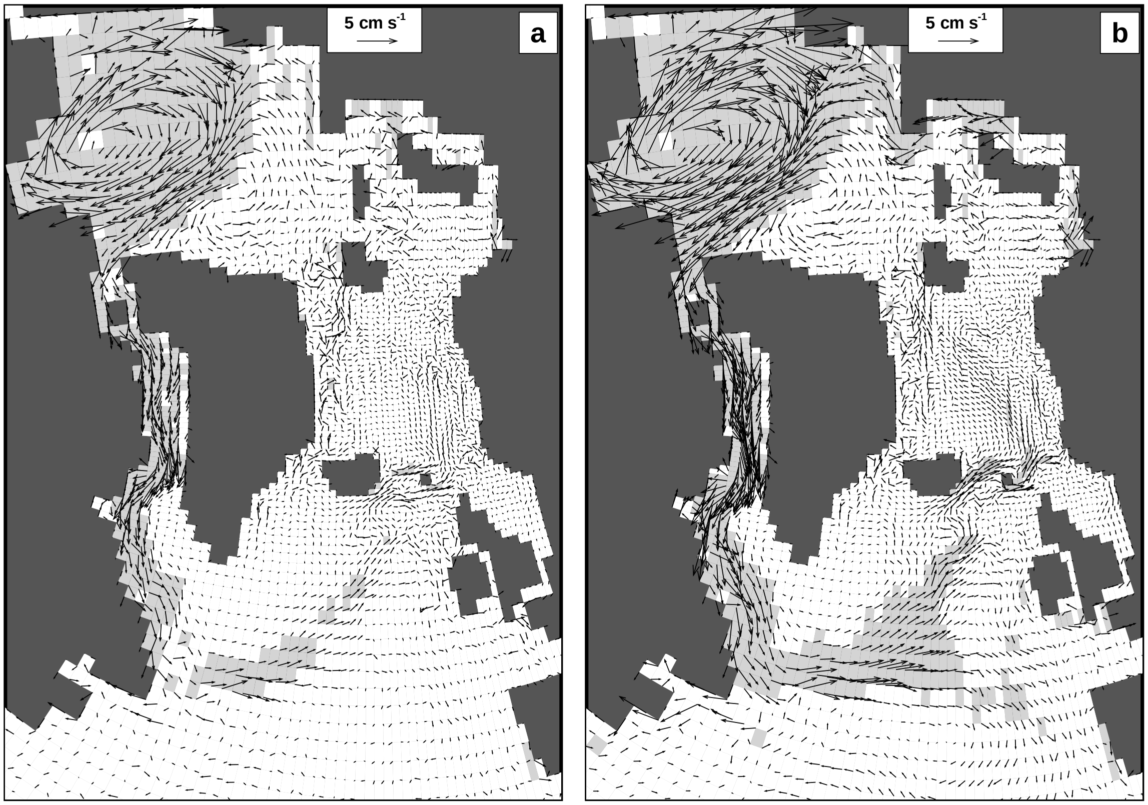

Figure 15: Difference compared to CTRL in the annual mean surface velocity (cm s^{-1}) in year 50 for (a) PX2 and (b) PX5. Shaded areas indicate an increase in absolute velocity greater than 1 cm s^{-1}.

1994; Latif et al. 2000; Räisänen 2001). Some of these models show a substantial reduction in AMOC with possible climatic impacts in northern Europe (e.g., Manabe and Stouffer 1994; Schiller et al. 1997; Cubasch et al. 2001; Vellinga and Wood 2002). However, in Latif et al. (2000), a different model response is found. Here, large-scale air-sea interactions in the tropics lead to anomalously high salinities in the tropical Atlantic. These anomalies are then advected northward into the sinking regions, thereby increasing the surface density and compensating the effects of the local warming and freshening. An alternative mechanism for maintaining the NAD is operating in the highly idealized model experiments presented here.

The obtained model results furthermore highlights the potential importance of the CA in controlling the freshwater budget of the Arctic and Atlantic Oceans, and thereby supporting the findings of Goosse et al. (1997). Coarse resolution ice-ocean and climate models are usually set up with a closed CA (e.g., Prange and Gerdes 1999; Rahmstorf 1999). However, several studies (e.g., Aagaard and Carmack 1989; Steele et al. 1996) suggest that the freshwater flux through this passage is larger than the one associated with the freshwater export through the Fram Strait. A closed CA will force the freshwater to escape through the Fram Strait, and possibly trigger a different ocean response to freshwater scenarios and/or reduced sea ice thickness than the one found in the present study. This underlines the need for representing this passage in global models used in climate studies.

An important limitation of this study is that it has been conducted under prescribed atmospheric conditions, which prevents any feedback mechanisms between the ice-ocean system and the atmo-

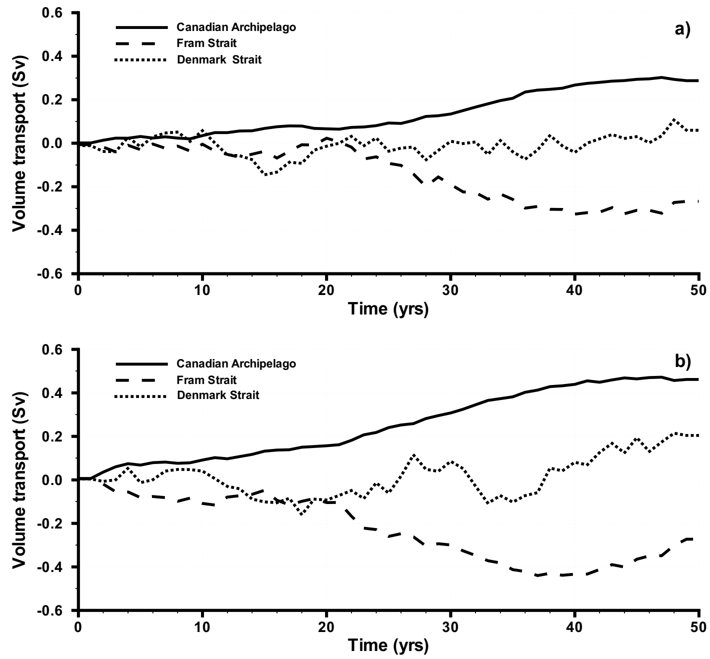

Figure 16: Time series showing the difference compared to CTRL in the annual mean net southward volume transport (Sv) for (a) PX2 and (b) PX5 through the CA (solid line), Fram Strait (dashed) and Denmark Strait (dotted). Negative values indicate reduced transport.

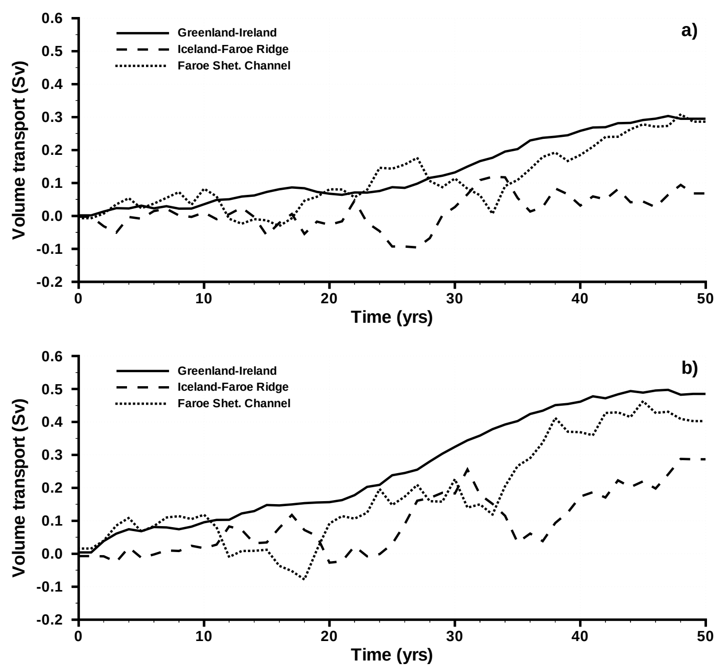

Figure 17: Time series showing the difference compared to CTRL in the annual mean net northward volume transport (Sv) for (a) PX2 and (b) PX5 through the GI section (solid line), the IFR (dashed) and the FSC (dotted). Negative values indicate reduced transport.

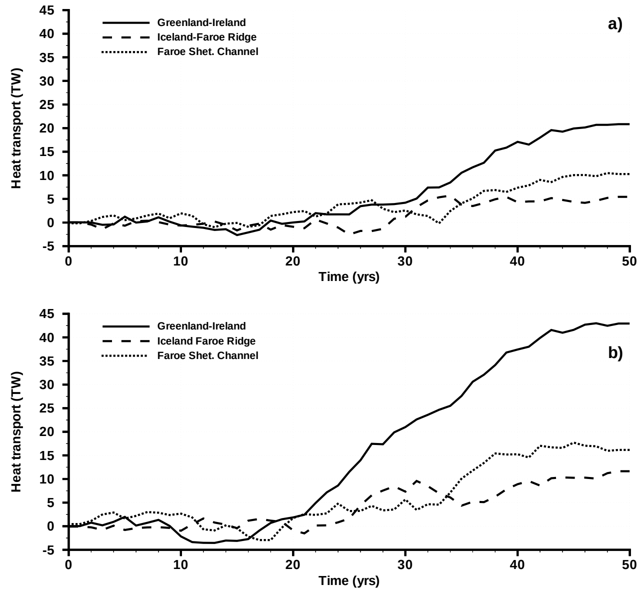

Figure 18: Time series showing the difference compared to CTRL in the annual mean net northward heat transport (TW) for (a) PX2 and (b) PX5 through the GI section (solid), the IFR (dashed) and the FSC (dotted). Negative values indicate reduced transport.

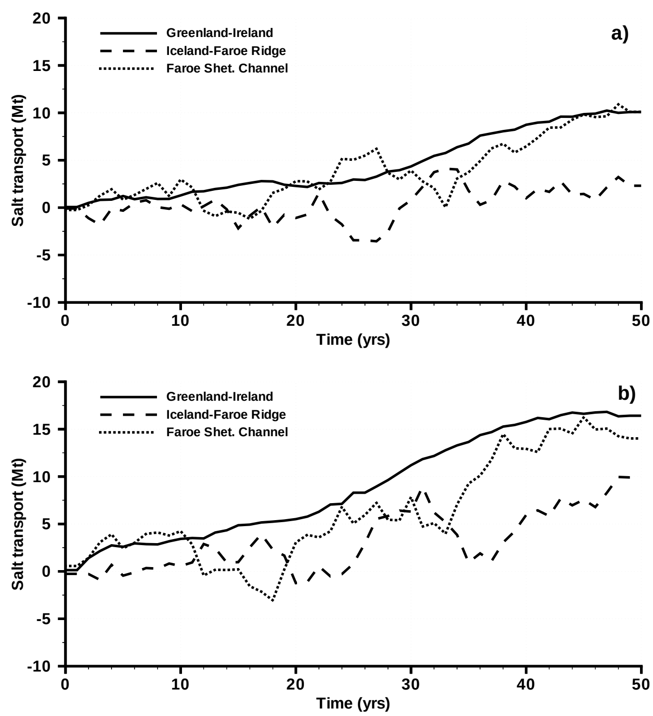

Figure 19: Time series showing the difference compared to CTRL in the annual mean net northward salt transport (Mt) for (a) PX2 and (b) PX5 through the GI section (solid), the IFR (dashed) and the FSC (dotted). Negative values indicate reduced transport.

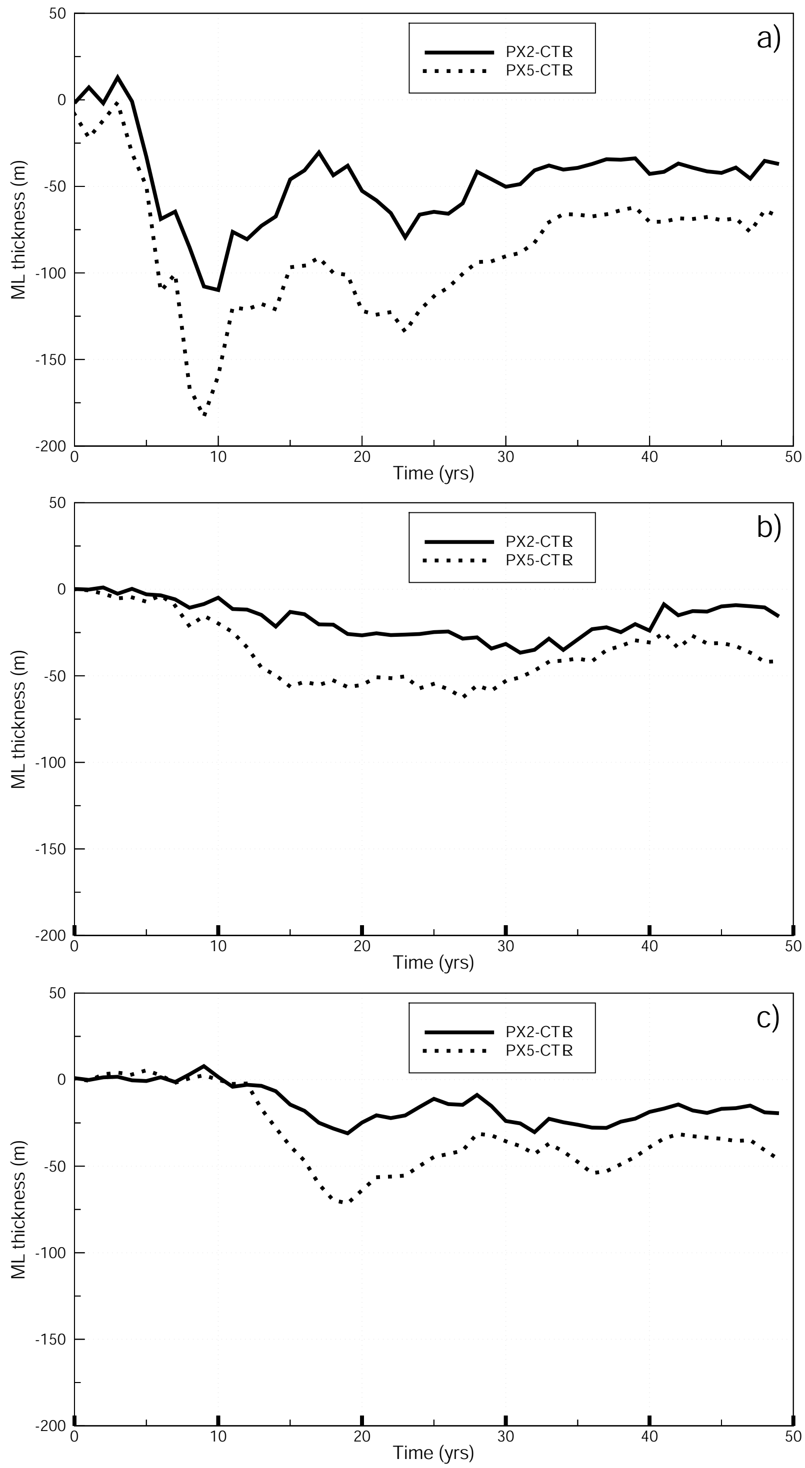

Figure 20: Time series showing the deviation in the winter time ML thickness (m) compared to CTRL for PX2 (solid line) and PX5 (dotted line) in the mixing regions of the model domain. (a) Labrador Sea, (b) Irminger Sea and (c) Greenland Sea.

sphere. For instance, one can expect that a modification of the NAD will affect air temperature and evaporation/precipitation in the Nordic Seas, which in turn may influence the atmosphere-ice-ocean system. Similar experiments with fully coupled atmosphere-sea ice-ocean models therefore need to be performed in order to test the response reported here. In fact, in a 150 years twin experiment with the Bergen Climate Model, a fully coupled atmosphere-sea ice-ocean climate model (Furevik et al. 2003), the poleward flow of Pacific water through the Bering Strait decreased, whereas the southward flow through the CA and the poleward flow through the FSC increased, in response to a three-fold increase in freshwater to the Nordic Seas and the Arctic Ocean (Otterå et al. 2003). These findings support the results presented here.

The presented study, although highly idealized and without any form of active atmospheric feedback mechanisms, indicate that increased freshwater supply to the Arctic – also in combination with reduced sea ice thickness in the Arctic – do not necessarily have a one-way negative feedback on the NAD, at least on multi-decadal time scales.

7 Summary

A 3-D isopycnic coordinate OGCM coupled to dynamic and thermodynamic sea ice modules has been used to examine the combined effect of increased freshwater flux to, and reduced sea ice thickness within, the Arctic Ocean. Two 50 years perturbation simulations are examined - one with a doubling of the modern Arctic river runoff, and a second, more extreme case, where the river runoff is five times the modern. It has been assumed that the additional supply of freshwater follows from a warmer climate. The heat associated with this warming has been applied to the model system by reducing the simulated sea ice thickness.

For both simulations, the modelled ocean response is qualitatively the same: The Arctic and North Atlantic SSS are reduced, leading to an initial weakening of the NAD. The freshening of the surface waters in the Arctic leads to increased density gradients in the central Arctic Ocean. This, together with increased momentum transfer across the thinner sea ice, lead to an intensified BG, which in turn increases the volume transport through the CA. To compensate for this southward transport of mass, more of the warm and saline Atlantic waters are carried northward with the NAD. The increased transport of salt to the northern North Atlantic and the Nordic Seas thus counteract the impact of the increased freshwater runoff to the Arctic, and tends to stabilize the NAD.

The presented study has focused on the circulation and the thermodynamics of the North Atlantic-Arctic climate system. A continuation of the study is planned with a global coupled atmosphere-ocean model, where the NAD and the AMOC can be studied on centennial time scales. Such studies will be useful to examine theories on glacial circulation, to identify the origin, propagation and decay of dynamic and thermodynamic anomalies in the Atlantic-Arctic region, and to further explore the role of flow of water through the CA in climate studies.

Acknowledgements

This study has been supported by the Research Council of Norway through the project A Model Study of the Glacial Circulation and Biogeochemistry with Focus on the High Northern Seas (Project No. 134542/720), the RegClim project, and the Program of Supercomputing. The support from the G. C. Rieber Foundations is highly acknowledged.

References

Aagaard K, Carmack EC (1989) The role of sea ice and other fresh water in the Arctic Circulation. J Geophys Res 94:14485–14498

Anderson LG, Björk G, Holby O, Jones EP, Kattner G, Koltermann KP, Liljeblad B, Lindegren R, Rudels B, Swift J (1994) Water masses and circulation in the Eurasian Basin: Results from the *Oden* 91 expedition. J Geophys Res 99:3273–3283

Aukrust T, Oberhuber JM (1995) Modelling of the Greenland, Iceland and Norwegian Seas with a coupled sea ice - mixed layer - isopycnal ocean model. J Geophys Res 100:4771–4789

Bleck R, Rooth C, Hu D, Smith LT (1992) Salinity-driven Thermocline Transients in a Wind- and Thermohaline-forced Isopycnic Coordinate Model of the North Atlantic. J Phys Oceanogr 22:1486–1505

Broecker WS, Bond WS, McManus G, Klas M, Clark E (1992) Origin of the North Atlantic's Heinrich events. Climate Dyn 6:265–273

Carmack EC (1990) Large-Scale Physical Oceanography of Polar Oceans, in: Polar Oceanography, Part A: Physical Scienxce, ed. Smith WO, Academic Press, Inc., San Diego, California, pp. 171–222

Clark PU, Pisias NG, Stocker TF, Weaver AJ (2002) The role of the thermohaline circulation in abrupt climate change. Nature 415:863–869

Cooper C, Gordon C (2002) North Atlantic Ocean decadal variability in the Hadley Centre Coupled Model. J Climate 15:45–72

Cubasch U, Meehl GA, Boer GJ, Stouffer RJ, Dix M, Noda A, Senior CA, Raper S, Yap KS (2001) Projections of future Climate Change, in: Climate Change 2001: The Scientific Basis: Contribution of Working Group I to the Third Assesment Report of the Intergovernmental Panel on Climate Change, eds. Houghton JT, Ding Y, Griggs DJ, Noguer M, der Linden PJV, Dai X, Maskell K, Johnson CA, Cambridge University Press, Cambridge, New York, pp. 526–582

Drange H, Simonsen K (1996) Formulation of Air-Sea Fluxes in the ESOP2 Version of MICOM, Tech. Rep. 125, Nansen Environmantal and Remote Sensing Center, Bergen, Norway

Dümenil L, Isele K, Liebscher HJ, Schröder U, Wilke K (1993) Discharge data from 50 selected rivers for GCM validation, Tech. Rep. 100, Max Planck Institute, Hamburg, Germany

ECMWF (1988) ECMWF forecast model. Physical parametrization, Research Manual 3, 2nd Edition, 1/88

Fairbanks RG (1989) A 17,000-year glacio-eustatic sea level record: Influence of glacial melting rates on the Younger Dryas event and deep-ocean circulation. Nature 342:637–642

Furevik T, Bentsen M, Drange H, Kindem IKT, Kvamstø NG, Sorteberg A (2003) Description and validation of the Bergen Climate Model: ARPEGE coupled with MICOM. Climate Dyn 21:27–51, doi:10.1007/s00382-003-0317-5

Gent PR (2001) Will the North Atlantic Ocean thermohaline circulation weaken during the 21st century? Geophys Research Letters 28:1023–1026

Goosse H, Fichefet T, Campin JM (1997) The effects of the water flow through the Canadian Archipelago in a global ice-ocean model. Geophys Research Letters 24:1507–1510

Hansen B, Malmberg S, Saelen OH, Osterhus S (1998) Measurment of flow north of the Faroe Islands June 1986, in: ICES Cooperative Research Report nr. 225, The ICES NANSEN Project, Copenhagen

Hansen B, Østerhus S (2000) North Atlantic - Nordic Seas exchanges. Prog of Oceanography 45:109–208

Harder M (1996) Dynamik, Rauhigkeit und Alter des Meereises in der Arktis, Ph.D. thesis, Alfred-Wegner-Institut für Polar- und Meeresforschung, Bremerhaven, Germany

Hibler WD (1979) A dynamic thermodynamic sea ice model. J Phys Oceanogr 9:815–846

Hopkins TS (1991) The GIN Sea - A synthesis of its physical oceanography and litterature review 1972-1985. Earth Science Reviews 30:175–318

Huschke RE (1969) Arctic cloud statistics from air calibrated surface weather observations. Memo, Tech. Rep. RM-5003-PR, Rand. Corporation, Santa Monica, Calif.

Johannessen OM, Miles M (2000) Arctic sea ice and climate change - will the ice disappear in this century? Science Prog 83(3):209–222

Johannessen OM, Shalina EV, Miles M (1999) Satellite evidence for an Arctic sea ice cover in transformation. Science 286(5446):1937–1939

Jones GA, Keigwin LD (1988) Evidence from Fram Strait (78°N) for early deglaciation. Nature 336:56–59

Kreyscher M, Harder M, Lemke P, Flato GM (2000) Results of the Sea Ice Model Intercomparison Project: Evaluation of sea-ice rheology schemes for use in climate simulations. J Geophys Res 105:11299–11320

Latif M (1998) Dynamics of interdecadal variability in coupled ocean-atmosphere models. J Climate 11:602–624

Latif M, Roeckner E, Mikolajewicz U, Voss R (2000) Tropical stabilization of the thermohaline circulation in a greenhouse warming simulation. J Climate 13:1809–1813

Legates DR, Willmott CJ (1990) Mean seasonal and spatial variability in gauge-corrected, global precipitation. Int J Climatol 10:111–127

Lehman SJ, Keigwin LD (1992) Sudden changes in North Atlantic circulation during the last deglaciation. Nature 356:757–762

Levitus S, Boyer TP (1994) World Ocean Atlas 1994, Volume 4: Temperature, NOAA Atlas NESDIS 4, Washington, D.C., 117pp

Levitus S, Burgett R, Boyer TP (1994) World Ocean Atlas 1994, Volume 3: Salinity, NOAA Atlas NESDIS 3, Washington, D.C., 99pp

Manabe S, Stouffer RJ (1994) Multiple-century response of a coupled ocean-atmosphere model to an increase of atmospheric carbon dioxcide. J Climate 7:5–23

Maykut GA (1978) Energy exchange over young sea ice in the Central Arctic. J Geophys Res 83:3646–3658

Millero FJ (1978) Freezing point of seawater, in: Eighth Report on the Joint Panel on Oceanographic Tables and Standards, UNESCO, Paris, UNESCO Tech. Pap. Mar. Sci. No. 28, Annex 6

Mitchell JFB, Johns TC, Gregory JM, Tett SFB (1995) Climate response to increasing levels of greenhouse gases and sulphate aerosols. Nature 376:501–504

Mosby H (1962) Water, salt and heat balance of the North Polar Sea and the Norwegian Sea. Geophys Norv 24(11):289–313

Oberhuber JM (1988) An atlas based on the 'COADS' data set: The budgets of heat, buoyancy and turbulent kinetic energy at the surface of the global ocean, Tech. Rep. 15pp, Max Planck Institute, Hamburg, Germany

Otterå OH, Drange H, Bentsen M, Kvamstø NG, Jiang D (2003) The sensitivity of the present day Atlantic meridional overturning circulation to freshwater forcing. Geophys Research Letters 30(17):1898, doi:101029/2003GL017578

Peltier WR (1994) Ice age paleotopography. Science 265:195–201

Peterson BJ, Holmes RM, McClelland JW, Vorosmarty CJ, Lammers RB, Shiklomanov AI, Shiklomanov IA, Rahmstorf S (2002) Increasing river discharge to the Arctic Ocean. Science 298 (5601):2171–2173

Prange M, Gerdes R (1999) Influence of Arctic river runoff on the circulation in the Arctic Ocean, the Nordic Seas and the North Atlantic. ICES ASC Council Meeting L/11:5 pp

Rahmstorf S (1995) Climate drift in an ocean model coupled to a simple, perfectly matched atmosphere. Climate Dyn 11:447–458

Rahmstorf S (1999) Long-term global warming scenarios computed with an efficient coupled climate model. Climatic Change 43:353–367

Räisänen J (2001) CO_2-induced climate change in the Arctic area in the CMIP2 experiments. SWECLIM Newsletter 11:23–28

Roach AT, Aagaard K, Pease CH, Salo SA, Weingartner T, Pavlov V, Kulakov M (1995) Direct measurements of transport and water properties through the Bering Strait. J Geophys Res 100:18443–18457

Roullet G, Madec G (2000) Salt conservation, free surface, and varying levels: a new formulation for ocean general circulation models. J Geophys Res 105:23927–23942

Rudels B, Anderson LG, Jones EP (1996) Formation and evolution of the surface mixed layer and halocline in the Arctic Ocean. J Geophys Res 101:8807–8821

Schiller A, Mikolajewicz U, Voss R (1997) The stability of the North Atlantic thermohaline circulation in a coupled ocean-atmosphere general circulation model. Climate Dyn 13:325–347

Semtner AJ (1987) A numerical study of the sea ice and ocean circulation in the Arctic. J Phys Oceanogr 17:1077–1099

Simonsen K (1996) Heatbudgets and freshwater forcing of the Nordic Seas and the Artic Ocean, Ph.D. thesis, Nansen Env. and Remote Sensing Center, Bergen, Norway, September, 1996

Simonsen K, Drange H (1997) Surface forcing and initialization of the ESOP2 version of MICOM, Tech. Rep. 116, Nansen Environmantal and Remote Sensing Center, Bergen, Norway

Simonsen K, Haugan PM (1996) Heat budgets of the Arctic Mediterranean and sea surface heat flux parametrizations for the Nordic Seas. J Geophys Res 101:6553–6576

Steele M, Thomas D, Rorhrock D (1996) A simple model study of the Arctic Ocean freshwater balance, 1979-1985. J Geophys Res 101:20833–20848

Sun S, Bleck R (2001) Atlantic Thermohaline Circulation and its Response to Increasing CO_2 in a Coupled Atmosphere-Ocean Model. Geophys Research Letters 28:4223–4226

Timmermann A, Latif M, Voss R, Grötzner A (1998) Northern hemisphere interdecadal variability: A coupled air-sea mode. J Climate 11:1906–1931

Vellinga M, Wood RA (2002) Global climatic impacts of a collapse of the Atlantic thermohaline circulation. Climatic Change 54:251–267

Vinnikov KY, Robock A, Stouffer RJ, Walsh JE, Parkinson CL, Cavalieri DJ, Mitchell JFB, Garrett D, Zakharov VF (1999) Global warming and Northern Hemisphere ice extent. Science 286:1934–1937

Walsh JE, Johnson CM (1979) An analysis of Arctic ice fluctuations, 1953-77. J Geophys Res 9:580–591